Development and integration of an autopilot system for a full-sized aircraft using open-source UAV technology

Kabelo Mpurwana[1*], *Russell* Phillips[1], and *Theo* van Niekerk[2]

[1]Nelson Mandela University, Department of Mechanical Engineering, Gqeberha, South Africa
[2]Nelson Mandela University, Department of Mechatronic Engineering, Gqeberha, South Africa

Abstract. This study presents the integration and validation of an open-source autopilot system for a full-sized motor glider, demonstrating its suitability for autonomous operations. The Whisper motor glider was retrofitted with a Cube Orange flight controller running ArduPlane, and control force measurements were used to size actuators and inform system tuning. A structured approach, which combined control force characterization, SITL simulation, and progressive flight testing, was used to configure and refine the system. Autonomous missions were successfully executed, with an average flight path tracking error of 1.75 m between waypoints and an altitude error of 28.7 m. The results confirm the feasibility of adapting manned aircraft for autonomous flight using low-cost, open-source tools, offering a practical foundation for high-endurance UAV applications.

1 Introduction

South Africa's coastline stretches over 3000 km, with a maritime zone exceeding three times its landmass. These regions are vital to national development, as emphasized in the National Development Plan, which identifies the ocean economy as a key driver of job creating and economic growth [1, 2]. However persistent threats such as illegal fishing, piracy, and smuggling compromise national security and sustainability [2, 3].

In the absence of a dedicated coast guard, the responsibility for maritime patrol and search operations falls to the South African Air Force (SAAF). Due to ongoing budgetary constraints, the SAAF relies on aging Douglas C-47TP aircraft, platforms that are well beyond their intended service life but remain the only ones in the fleet with sufficient endurance for maritime surveillance. This capability gap underscores the need for a cost-effective, high-endurance surveillance solution [4, 5].

Unmanned aerial systems (UAS) offer several advantages for maritime surveillance, including extended endurance, persistent area coverage, and reduced risk to human operators. Their adoption in developed countries has accelerated due to improvements in control systems, miniaturized avionics, and growing acceptance of civil airspace integration [6-8].

* Corresponding author: kabelo.mpurwana@mandela.ac.za

These advancements have significantly lowered development barriers, making sophisticated UAV capabilities accessible at reduced cost.

Nonetheless, airframe development remains a key barrier to large-scale UAV deployment in resource-limited settings. The certification of new aircraft demands substantial investment and carries technical and regulatory risk. A pragmatic solution is to retrofit proven and appropriate airframes with autonomous control systems, enabling safe, cost-effective development with the option of manned oversight during testing.

1.1 Related work

A number of UAS platforms have adopted the retrofit approach, leveraging certified or proven manned aircraft to accelerate development, reduce cost, and overcome regulatory constraints. One example is the Centaur optionally piloted aircraft, developed by Aurora Flight Sciences, using a Diamond DA42 twin-engine general aviation platform. The aircraft supports a range of mission-specific payloads, including maritime search radars and communication relays, and offers an endurance of up to 24 hours with a range of approximately 3700 km [9].

A similar effort was undertaken by Mississippi State University's Raspet Flight Research Laboratory and Navmar Applied Sciences Corporation with the development of the Teros UAV based on the Sonex Xenos-B motor glider [10]. The Xenos-B was selected for its favourable aerodynamic efficiency, low empty weight, and high endurance potential. The resulting platform, Teros, features a wingspan of nearly 12 metres, 270-kilogram payload capacity, and a maximum endurance exceeding 24 hours. Designed to support a range of research and operational missions, including disaster response and environmental monitoring, the Tero illustrates how an experimental-category aircraft can be successfully converted into a large-scale unmanned system [11].

Another notable example is the Safran Patroller™, a medium- to long-range UAV operated by the French Army for intelligence, surveillance, and reconnaissance (ISR) missions. The system is based on the Ecarys ES15 motor glider airframe and incorporates a modular payload architecture and satellite communication capability, enabling operations exceeding 1000 km [12, 13].

These examples demonstrate the viability of converting suitable manned aircraft for autonomous use. Motor gliders, with their aerodynamic efficiency and low fuel consumption, are ideal for persistent surveillance and offer sufficient internal volume for flight systems and payloads. For budget-constrained institutions, such conversions provide a cost-effective path to capable UAV development with reduced time and certification requirements.

1.2 Research objectives

The objective of this study was to develop and evaluate an open-source autopilot system capable of autonomously controlling a full-sized motor glider, serving as a prototype for a low-cost, high-endurance UAV for maritime surveillance. The system was designed to command only the primary control surfaces (aileron, elevator, and rudder), with throttle and secondary systems managed by a test pilot to ensure safety during flight testing.

A staged development approach was followed, beginning with bench integration, simulation-based tuning, and culminating in full-scale flight trials. This progression enabled safe, incremental validation of the system under increasingly realistic conditions. System performance was assessed using two primary metrics, flight path tracking accuracy and altitude control. These metrics reflect the system's ability to maintain stable, precise navigation which is crucial for autonomous mission execution in variable atmospheric conditions.

2 System architecture

This section outlines the aircraft platform, the actuator selection and integration, and the chosen autopilot hardware and software stack used to enable autonomous flight.

2.1 Airframe overview

Fig. 1. Whisper motor glider.

The test platform for this study was the Whisper motor glider (Fig. 1), a two-seat, side-by-side composite aircraft designed for the homebuilder market. Its low construction and operating cost make it well-suited for UAV conversion. The airframe supports multiple engine options, including Rotax, Limbach, and Jabiru, many of which run on automotive fuel, reducing reliance on expensive and less accessible 100 LL AVGAS. Key specifications are shown in Table 1.

Table 1. Whisper motor glider specifications.

Parameter	**Value**	**Performance**	**Value**
Wingspan (m)	16	$V_{vertical}$ (m/s)	3.6
Wing area (m^2)	15	$V_{max\ level}$ (km/h)	210
Length (m)	7.16	V_{cruise} (km/h)	*189*
Empty weight (kg)	530	V_{NE} (km/h)	*250*
Max takeoff weight (kg)	775	V_A (km/h)	160
Fuel capacity (*l*)	85	Fuel consumption(cruise) (l/h)	12

2.1.1 Flight control system and servo sizing

The Whisper motor glider employs a conventional mechanical flight control system. The elevator and rudder are actuated via flexible steel cables, while the ailerons are operated through a combination of pushrods and a differential bellcrank mechanism. To reduce adverse yaw, the aileron system incorporates differential deflection, wherein the upward-deflecting aileron moves through a greater angle than its downward counterpart. This differential is achieved mechanically at the bellcrank, simplifying the setup of the autonomous actuators.

To appropriately size the servos for autonomous control, it was necessary to measure the in-flight control forces applied by the pilot. Strain gauges were installed on the control stick to quantify the pitch and roll forces required to manoeuvre the aircraft. Four 6mm, 120-ohm linear strain gauges were arranged in two half-bridge configurations to independently capture bending strains in the lateral (roll) and longitudinal (pitch) directions as illustrated in Fig. 2. The control stick is constructed from 4130 chromoly steel, and its elastic behaviour is assumed to be linear within the measured range.

Fig. 2. Control stick load cell.

The stress (σ) at each strain gauge location was determined from the measured strain (ε) and the Modulus of elasticity (E) of the control stick (Hooke's Law):

$$\sigma = E\epsilon \tag{1}$$

The corresponding bending moment (M) was calculated using the section modulus (I_{yy}/y) of the stick cross-section:

$$M = \frac{\sigma I_{yy}}{y} \tag{2}$$

Finally, the force transmitted through the control cables was calculated from the bending moment and the perpendicular distance ($\bar{x}$) to the cable attachment point:

$$F_{cable} = \frac{M}{\bar{x}} \tag{3}$$

Control force measurements were limited to the elevator and aileron axes. The rudder system's mechanical layout, with its flexible cable routing and coupled co-pilot pedals, made it difficult to identify a mounting location for the strain gauges that provided both sufficient structural integrity and accurate measurement of the control forces. Moreover, the rudder's critical design consideration was not the control force magnitude but the actuation speed, particularly during ground roll and takeoff, where rapid and precise rudder input is required to counter the aircraft's left-turning tendency from propeller effects. This tendency is especially pronounced in aircraft with conventional gear, due to the gyroscopic precession. Therefore, actuator selection for the rudder prioritized responsiveness over force capacity.

2.2 Autopilot software

Selection of the autopilot suite was based on both the airframe's technical requirements and the maturity, community support, and adoption of available systems. A comparative survey by Ebeid et al [14] identified ArduPilot and PX4 as the most advanced open-source platforms, both offering multi-mode support, broad sensor compatibility, and built-in fault detection. While PX4 is often favoured for its flexibility, ArduPilot's frame-specific firmware simplifies configuration, making it particularly well-suited to conventional aircraft like the Whisper motor glider.

The core architecture of an ArduPilot-based system is shown in Fig. 3. Control can be achieved either through a standard RC radio or via MAVLink, a lightweight protocol designed for efficient onboard and offboard communication [15].

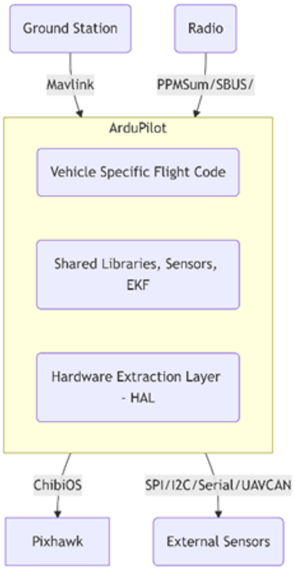

Fig. 3. ArduPilot basic structure adapted from [16].

2.2.1 ArduPlane control architecture

The ArduPlane firmware (v4.1.2 - 20416B38) uses a hierarchical control architecture comprising high-level navigation and altitude controllers and low-level attitude controllers as shown in Fig. 4.

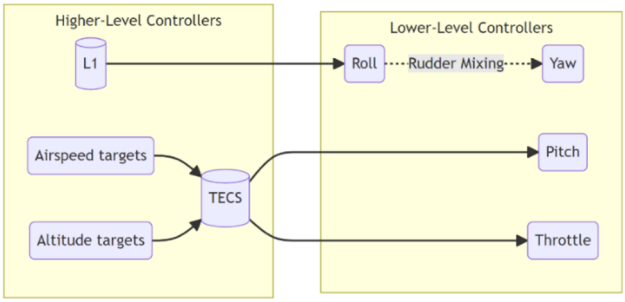

Fig. 4. ArduPlane controllers adapted from [16].

Lateral navigation is managed by the L1 controller, which calculates lateral acceleration commands to keep the aircraft on a straight-line path between GPS waypoints. It translates geodetic positions into navigable vectors and determines the horizontal acceleration need to stay on course. Based on the work of Park et al. [17], the modified controller supports user-level tuning but does not include an explicit integral term, relying on the inner attitude and rate loops for bias correction. Altitude and airspeed are jointly managed by the Total Energy Control System (TECS), which regulates pitch and throttle to control the aircraft's total energy. Throttle adjusts the total energy level, while elevator inputs shifts energy between speed and altitude, allowing coordinated control without decoupling the axes [18].

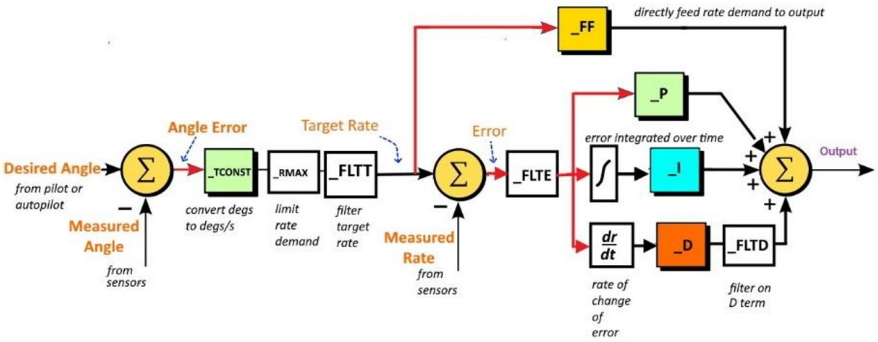

Fig. 5. ArduPlane PID controller [16].

ArduPlane uses cascaded PID controllers (Fig. 5) to regulate roll and pitch beneath the navigation and energy management layers. The system calculates the angular error between commanded and measured attitudes, converts it into a rate target constrained by user-defined limits (RMAX), and passes it to an inner PID loop. This loop compares the target with measured body rates, and its output is combined with a feedforward term that accounts for aerodynamic damping. The feedforward input provides most of the control action, while the PID terms correct for residual errors caused by disturbances or unmodelled dynamics. User-adjustable low-pass filter are available to tune responsiveness and supress noise [16, 18].

Yaw control is handled separately and serves as both a yaw damper and a sideslip controller. It produces coordinated turns by applying rudder deflection proportionally to aileron input and minimizes lateral accelerations to eliminate sideslip. This improves directional stability and overall handling, particularly during critical phases of flight and in crosswind conditions.

To maintain consistent handling across varying airspeeds, ArduPlane scales control outputs based on dynamic pressure. Larger deflections are applied at low speeds, while smaller inputs suffice at higher speeds. This compensation ensures predictable control behaviour through the aircraft's flight envelope.

2.3 Autopilot hardware

The autopilot system was built around the Cube Orange flight controller, a robust and widely supported platform capable of running ArduPilot firmware. It features triple-redundant IMUs, isolated vibration-damping, and a high performance H7 processor with a dedicated failsafe co-processor. A Here3 GNSS and compass module was installed for position and heading estimation, and a digital differential airspeed sensor was connected to the aircraft's existing Pitot-static system. The system was powered separately through a 3-cell Li-Po battery. A summary of the key onboard hardware is provided in Table 2.

Table 2. Autopilot system hardware components.

Component	**Description**	
Flight controller	Cube Orange Standard Set	
GNSS module	Here3 with u-blox M8P receiver, magnetometer, RTK support	
Airspeed sensor	Pix32	
Remote control	FrSky Taranis QX7 with X8R receiver	
Power Supply	Avionics	3S 2300 mAh Li-Po
	Actuators	2S 20 Ah Li-Po

As the autopilot did not control the throttle, a visual feedback system was implemented to relay throttle commands to the onboard test pilot. A microcontroller read the autopilot's PWM throttle output and drove an LED strip, where the number of illuminated LEDs indicated the commanded throttle level during autonomous flight.

Servo selection was based on torque, speed and cost. Commercial aviation servos were ruled out due to compatibility and price. Instead, high-torque Hiwonder 60MG servos were used. These provided 60 kg.cm of torque at 7.4 V and were mechanically linked for the required control authority. The final setup included two pairs of servos for the elevator and two banks of three for the rudder and ailerons. Throw was based on stick displacement, with software limits to prevent overtravel. Instead of steel cables, 4mm high-strength dinghy line was used for its low stretch and high strength.

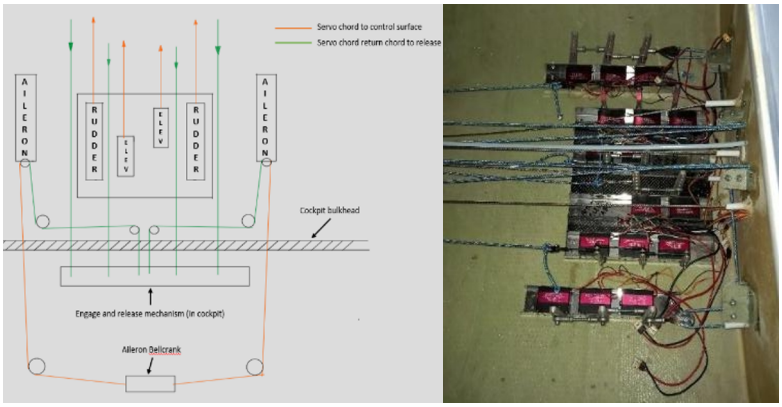

Fig. 6. Servo layout and installation.

To enable safe autonomous testing with full pilot override, a mechanical autopilot release system was implemented. Each servo bank was connected to a shared anchor plate mounted in the cockpit (Fig. 7). This plate could be disengaged in flight, releasing all servo lines and restoring manual control without added drag or binding. The design also allowed for pre-flight tension adjustments and provided a compact solution within the limited cockpit space.

Fig. 7. Autopilot release system.

3 Methodology

This section describes the staged methodology, beginning with a characterization flight to measure control forces, followed by simulation-based controller tuning and finally full-scale autonomous flight tests.

3.1 Characterization flight

The primary objective of the initial flight test was to quantify the pitch and roll control forces experienced during typical manoeuvres. This was achieved using the custom strain gauge-based control stick load cell (Fig. 2). Strain data was recorded using a P3 Strain Indicator and Recorder, while aircraft attitude, body rates, and airspeed data was logged via the Cube Orange flight controller and its external sensors. In addition to quantifying control forces, this flight was used to establish operational parameters for autopilot configuration. These included typical angular rates, attitude limits, and vertical speed ranges.

The flight plan was designed to capture the full range of pitch, roll, and yaw inputs experienced during general flight. It included:

- Takeoff and climb
- Shallow turns (<30° bank)
- Steep turns (>45° bank)
- Roll reversals (~80°)
- Pull-up/Pushover manoeuvres
- Slaloms and forward slips
- Approach and Landing

Each manoeuvre was executed with safety margins in place. Roll reversals and the pitch excursions were used to capture peak stick forces. The steep turns and slalom segment established the lateral control demands under various power settings, while climb-out and descent rates were used to define vertical speed limits.

All test flights were conducted under the South African Civil Aviation Authority's (SACAA) Part 94 Operation of Non-Type Certified Aircraft (NTCA) framework. A qualified test pilot remained in command throughout, and operations were carried out within a research and development context.

3.2 Software-in-the-loop (SITL) simulation

Prior to full-scale flight testing, the autopilot configuration and control strategies were evaluated using a Software-in-the-Loop simulation environment. ArduPilot SITL, run within Mission Planner, allows ArduPlane firmware to operate without physical hardware by receiving flight dynamics data from an external simulator. X-Plane 11 was selected as the simulation backend due to its blade element theory-based flight model, which provides high-fidelity handling characteristics for fixed-wing aircraft [16, 19].

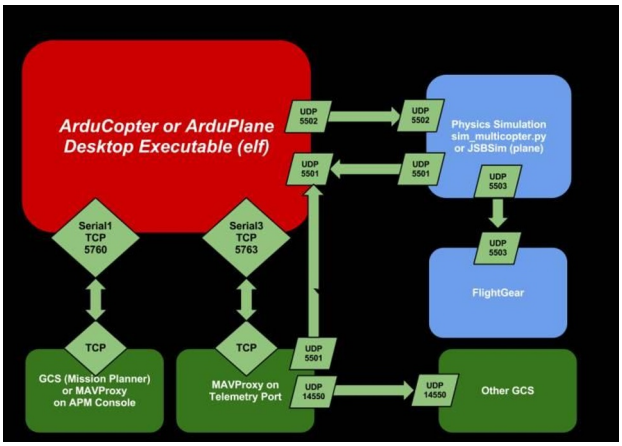

Fig. 8. ArduPilot SITL architecture [16].

The Cube Orange flight controller was emulated in the SITL environment, and RC inputs were provided via a joystick to replicate in-flight control conditions. To represent the Whisper motor glider, the Scheibe SF-25C Falke was used as a proxy, as it is a geometrically and aerodynamically similar as shown in Fig. 9. Both aircraft share comparable wingspan, length, and control surface configurations [20].

Fig. 9. Scheibe Falke (above) and Whisper motor glider.

3.2.1 SITL tuning

Following aircraft setup in SITL, tuning began with the low-level controllers in fly-by-wire (FBW-A) mode. FBW-A is an assisted mode that interprets pilot inputs as angle commands. The feedforward (FF) gains for the roll and pitch rate controllers were tuned first to ensure that the control surface deflections matched the commanded rates. Once the feedforward gains were fixed, the proportional and derivative feedback gains were incrementally tuned to refine the speed of response and reduce the overshoot. Integral gains were then introduced incrementally from zero, with small increases used to correct steady-state trim offsets while avoiding excessive low-frequency oscillations.

To complete the tuning of the lower-level controllers, the pitch-to-roll compensation (PTCH2SRV_RLL) and rudder coordination (KFF_RDDRIX) parameters were configured. These were adjusted to minimize altitude loss during turns and to maintain coordinated flight. Turning was validated using rapid roll manoeuvres and, with performance assessed through turn coordinator indications and altitude trends.

With the attitude controllers configured, navigation tuning focused on the NAVL1_PERIOD parameter, which sets the loop cycle time for the L1 controller, and the NAVL1_DAMPING parameter to stabilize path tracking between waypoints. A rectangular mission was used to evaluate turn entry, exit behaviour, and straight-line accuracy. Waypoint radius and bank angle limits were also adjusted to reduce overshoot.

TECS tuning was conducted in loiter mode, where the aircraft circles a fixed point at a defined altitude and radius (WP_LOITER_RAD). Altitude change commands were issued to assess climb and descent performance, constrained by bank angle (NAV_ROLL_CD) and navigation period settings. Key parameters of interest included:

- TECS_CLMB_MAX, TECS_SINK_MIN – for vertical speed limits.
- TECS_PITCH_MAX, TECS_PITCH_MIN – for pitch angle limits.
- TECS_SPDWEIGHT – for throttle/elevator coordination strategy.

This simulation process produced validated baseline settings and informed the safe configuration of the full-scale motor glider.

3.3 Full-scale flight testing and autonomous configuration

Following the simulation, the autopilot actuators were integrated into the Whisper motor glider. All primary control surfaces were actuated by digital servos connected through a mechanical release system, which allowed manual override in flight. System functionality and servo authority were first verified through ground tests and during manual test flights. Three control configurations were used throughout testing:

- Stick-and-rudder – traditional pilot control via the original cable system
- RC-mode – pilot inputs transmitted through the autopilot servos (with or without stabilization)
- Auto-mode – full autonomous control by the autopilot of the primary control surfaces.

Initial flights began in RC-mode, where controller response was evaluated during shallow turns and moderate pitch inputs. Simulation-derived parameters were used as a baseline and adjusted incrementally using flight log data. Focus was placed on refining the feedforward and damping terms for pitch and roll, and verifying yaw coordination and altitude stability.

Once stabilized flight was confirmed, the system was switched to auto-mode to execute waypoint missions. L1 controller parameters were evaluated for path-tracking performance. Altitude and airspeed control were tuned using TECS, with particular attention to TECS_SPDWEIGHT and the interaction between elevator and throttle authority.

A final test combined RC-mode takeoff with autonomous mission execution, validating servo performance under load and confirming that the autopilot could maintain airspeed, altitude, and path with acceptable deviations.

4 Results and discussion

This section presents the results of the system evaluation, including the performance analysis, control force measurements, simulation outcomes, and full-scale flight test findings.

4.1 Performance analysis of crew configurations

To evaluate the operational benefits of an unmanned configuration, a performance analysis was conducted using three crew-loading scenarios (two crew, one crew, and unmanned). The goal was to quantify the impact of crew weight on fuel load, endurance, and range. In all cases, a 16.8 kg payload, equivalent to a Wescam MX-10 imaging system, was included to simulate a maritime surveillance role[21]. The test aircraft, equipped with a 100 hp Rotax 912S engine, has an empty weight of 527.8 kg and a maximum takeoff weight of 775 kg. For this analysis, it is assumed that fuel capacity is limited by weight rather than volume, and each crew member weighs 80 kg. Table 3 summarizes the resulting fuel availability in each configuration.

Table 3. Crew configuration and fuel quantity.

Configurations	2 Crew	1 Crew	Unmanned
Crew weight (kg)	160	80	0
Fuel weight (kg)	70.4	150.4	230.4
Fuel volume (l)	98.5	210.3	322.2

Fuel consumption data at three cruise speeds, 100 km/h, 160 km/h, and 180 km/h, were sourced from engine charts[22] and verified through in-flight testing. These speeds correspond to low, medium, and high-power settings, respectively. Using the calculated fuel volumes and measured burn rates, endurance and range were computed and the data

presented in Fig. 10. As expected, removing crew significantly increase fuel capacity and, by extension, range and endurance. The unmanned configuration offers over three times the endurance of a two-crew configuration at lower cruise speeds. This highlights the potential of unmanned conversion to enhance mission duration and operational reach.

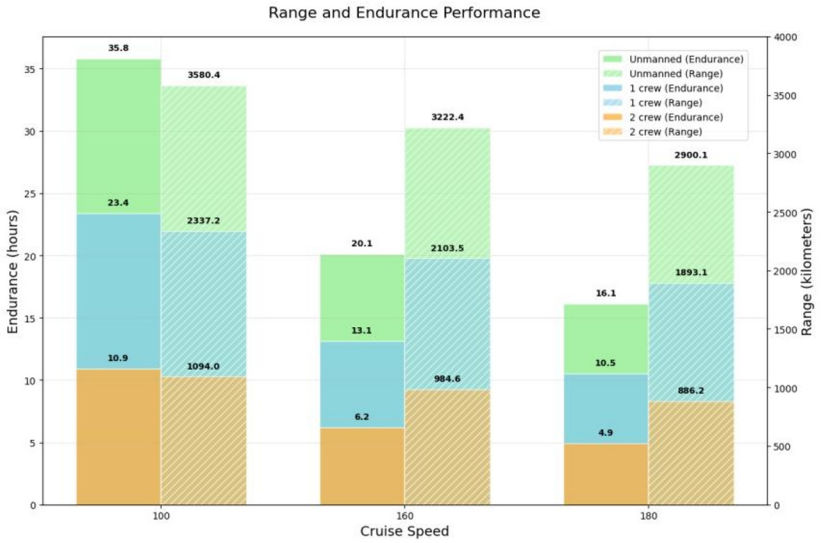

Fig. 10. Range and endurance performance.

4.2 Characterization flight test

This section presents the results from the characterization flight test which was conducted to inform actuator selection and establish operational standards and limits for the autopilot system.

4.2.1 Lateral control forces

Control forces for roll were derived from strain gauge measurements of the control stick, time-synchronized with flight attitude data. These forces included both aerodynamic hinge loads and mechanical control system loads. Peak forces occurred during high-deflection manoeuvres such as roll reversals and steep turns, with recorded values ranging from 25.2 N (left bank) to 29.5 N (right bank) as presented in Table 4.

Table 4. Roll forces.

Manoeuvres		**Force (N)**
Max Left Banking Force		-25.2
Max Right Banking Force		29.5
Shallow turn	*1*	-7.7
Roll reversal (80°)	*2*	26.9
Steep turn	*3*	-25.2
Forward slip	*4*	-15.4

Most lateral manoeuvres required less than 11 N, indicating that moderate roll inputs could be achieved with relatively low force. However, steep turns and roll reversals demonstrated the significantly higher demands that arise during dynamic manoeuvres. These

findings reinforced the need for adequate servo torque and rate authority to ensure the autopilot could respond effectively across the full operational envelope.

4.2.2 Longitudinal control forces

Key longitudinal control forces were evaluated during takeoff, pull-up/pushover manoeuvres, and forward slips. The highest elevator force recorded was 15.3 N prior to rotation (Fig. 11), coinciding with the tail being raised before takeoff. In the pull-up/pushover manoeuvre, peak forces of 9.8 N (push) and 10.9 N (pull) were observed, with a low average force of 4.3 N due to the steady control input.

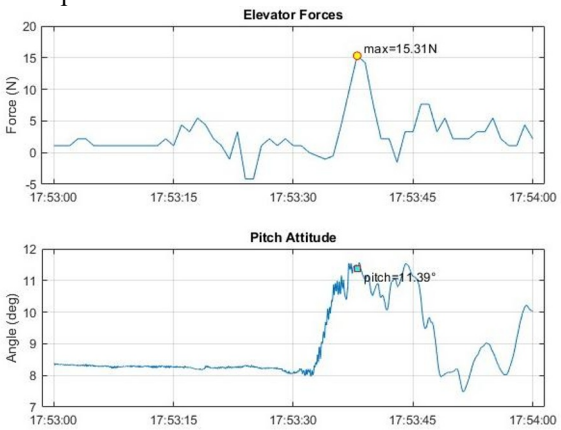

Fig. 11. Takeoff pitch force and attitude.

Overall, pitch control forces were lower than those required for lateral control, confirming the aircraft's higher sensitivity in the pitch axis. These results justified the use of more conservative tuning on the pitch controller and affirmed that moderate servo power was sufficient to meet longitudinal control demands under typical operating conditions.

4.2.3 Operational envelope definition

Operational parameters were derived from flight logs and manufacturer documentation to define safe limits for the autopilot. Maximum achieved roll and pitch angles, as well as typical attitudes during climb, descent, and approach are summarized in Table 5. Vertical speed and pitch/roll rates were extracted from GPS and IMU data, with average values used to set conservative controller targets.

Table 5. Operational parameters.

Parameter	**Value**
Max bank (symmetric)	50.0°
Max pitch (up/down)	12.4°/-11.3°
Climb pitch (130 km/h)	2.5°
Descent pitch (150 km/h)	-6.0°
Approach pitch (120 km/h)	-0.8°
Takeoff climb rate (mean)	2.7 m/s
Approach descent rate (mean)	-3.0 m/s
Vertical rate (max/min)	10.9/-8.0 m/s
Max roll rate (symmetric)	18.3 °/s
Mean roll rate (symmetric)	2.7 °/s

Max pitch rate (symmetric)	12.9 °/s
Mean pitch rate (symmetric)	2.5 °/s

To ensure safe autopilot operation and avoid aerodynamic stalls or over-speed conditions, conservative limits were adopted. The maximum bank angle was restricted to 25°, and pitch angles limited to 10°, up and down. These values were later changed as confidence in the system increased and higher limits were required for improved system performance.

4.3 SITL simulation

SITL tuning provided a controlled environment to refine the initial autopilot parameters and validate the tuning strategy before the full-scale integration. The most significant tuning outcomes were observed in the feedforward terms for pitch and roll, which had the greatest influence on achieving the desired response rates. While PID terms were also adjusted, their impact was less pronounced due to the inherent stability of the motor glider and higher aerodynamic damping modelled in the simulator.

Lower-level tuning confirmed that moderate to high feedforward values were required to achieved the desired roll response. The roll feedforward term was increased from 0.345 to 1.9, while the pitch term reduced from 1.0 to 0.8 to mitigate overshoots due to the aircraft's pitch sensitivity. Response times were defined as the time taken for the rate response to reach and remain within ±10% of the commanded value following a step input. Final response times of approximately 3 seconds in roll and 2.3 seconds in pitch closely matched those observed during the full-scale characterization flight.

Higher-level tuning focused on optimizing the NAVL1_PERIOD, NAVL1_DAMPING, and WP_RADIUS parameters to improve waypoint tracking. A maximum waypoint radius of 255 m was selected to allow smoother turn anticipation at cruise speeds of 160 km/h, thereby reducing path deviation at corner transitions. As expected, tracking errors peaked near the set radius during sharp turns, while between-waypoint deviations remained under 5 m, negligible for a 16-metre wingspan airframe.

TECS tuning in loiter mode revealed minor pitch oscillations during altitude transitions. This was attributed to overlapping control authority between throttle and elevator, governed by the selected TECS_SPDWEIGHT configuration. Despite these interactions, the aircraft maintained altitude effectively, and vertical speed targets were met without excessive pitch deviations.

Overall, SITL simulation validated the baseline control architecture and identified key tuning sensitivities, especially the influence of feedforward scaling and waypoint geometry. These insights directly informed the full-scale configuration and risk mitigation during early autonomous flight testing.

4.4 Full-scale flight test results

Following servo integration and in-flight verification of the autopilot release mechanism, initial testing was conducted in RC-mode using FBWA to validate simulation-based parameters. Shallow turns and moderate pitch changes confirmed that the system had sufficient control authority. Adjustments were made (Table 6), including increases in roll and pitch feedforward terms and reduction in P-gains. Final average response rates were 2.3 °/s in roll and 1.1 °/s in pitch. However, log analysis revealed low-frequency oscillations (±5° in roll and ±1° in pitch) likely due to servo trim mismatch and control line slippage.

Table 6. Parameter adjustments

Parameters		**Simulation**	**Motor Glider**
Roll	RLL_RATE_P	0.32	0.08
	RLL_RATE_I	0.08	0.15
	RLL_RATE_D	0.001	0.01
	RLL_RATE_FF	1.9	2.5
Pitch	PTCH_RATE_P	0.2	0.04
	PTCH_RATE_I	0.03	0.15
	PTCH_RATE_D	0.02	0.01
	PTCH_RATE_FF	0.8	1.2

The first autonomous mission consisted of 19 waypoints forming a closed loop at an altitude of 400 m. The mission was completed successfully, with an average lateral tracking error of 28.89 m between waypoints and an average altitude error of 36 m. Roll oscillations of up to 9.8° and altitude variations of 10 m were observed during turns.

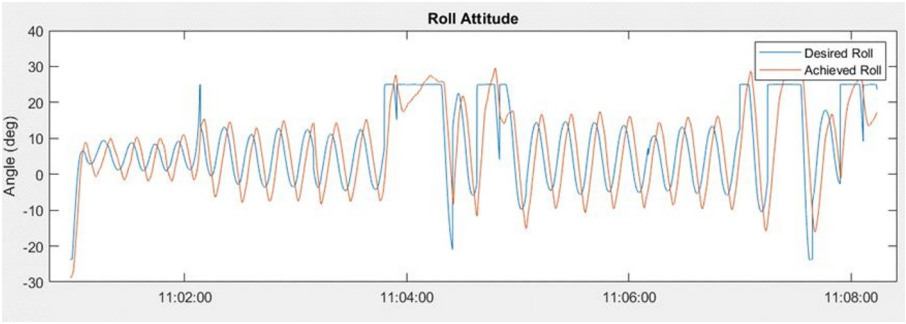

Fig. 12. Roll oscillations

Subsequent tuning focused on correcting flight controller mounting offsets, as the roll oscillations were centred around a consistent bias of approximately 5°, suggesting misalignment between the flight controller and the airframe. After adjusting the board offset parameters, path tracking improved, with average lateral error reduced to 14.52 m and altitude error to 20.72 m. However, roll oscillation persisted, now occurring closer to zero with slightly increased frequency, indicating improved symmetry but continued sensitivity in the control system.

To isolate the issue, the mission was replicated in SITL and similar oscillation could only be reproduced by lowering the loop cycle time to 12 seconds, suggesting that control loop cycling or servo positioning errors were plausible root causes. Further inspection indicated that the autopilot's neutral position often misaligned with the actual control surface trim, resulting in persistent corrections. These effects were exacerbated by control line slippage and tension variability. Because the L1 navigation controller does not include an integral term, steady-state biases of this nature were handled by the integral action in the inner roll loops. While this was tuned, tuning alone could not fully eliminate the observed behaviour.

Fig. 13. Final waypoint mission.

A final test flight was conducted using an RC-mode takeoff followed by autonomous mission execution. This approach was adopted after several preparatory flights were completed to build confidence in the system's behaviour at low speeds. Testing in this manner allowed the servo and control surface trims to be aligned on the ground prior to takeoff. The mission (Fig. 13) included shallow and medium turns and staged a descent into a long straight-in approach for landing. The autopilot remained engaged until 78m above the ground, at which point it was disengaged and the landing performed manually.

The results showed significant improvements (Fig. 14) with an average flight path error of 11.3 m, and inter-waypoint tracking error reduced to 1.75 m. Airspeed and altitude performance were consistent with mission targets, with average deviation of 18.4 km/h and 28.7 m respectively. These remained well within acceptable margins given the aircraft's cruise speed of 160 km/h at 400 m altitude.

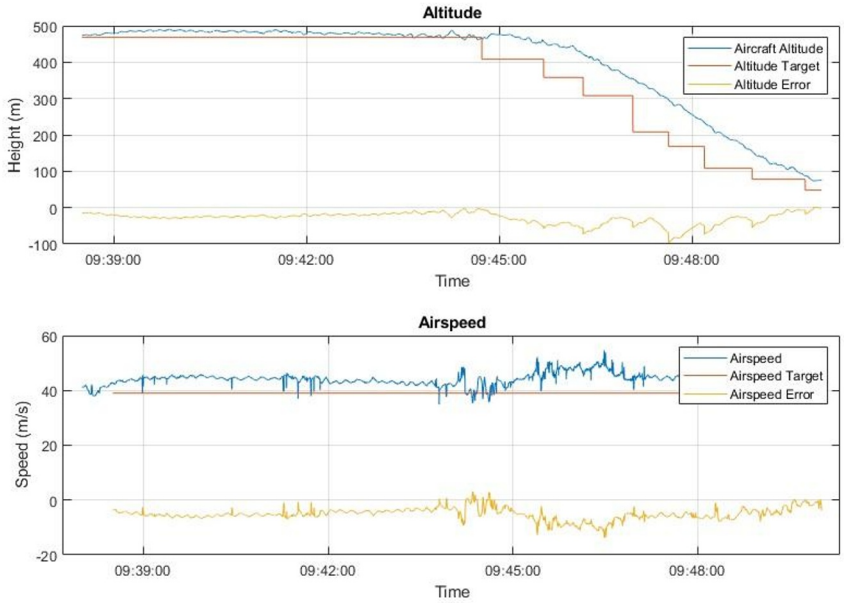

Fig. 14. TECS errors.

Log analysis showed roll oscillations (Fig. 15) with an amplitude of 1.6° and a period of 11 seconds. These oscillations were small enough to go unnoticed by the pilot during flight and did not affect the aircraft's ability to follow the planned flight path. They suggest an overactive controller attempting to correct minor perturbations that would otherwise have

been damped out by the airframe's inherent stability. The persistence of a small limit cycle is therefore attributed to a combination of linkage variability and the conservatively tuned inner loop integrators, highlighting the need for refined I-gain tuning and potential mechanical adjustments.

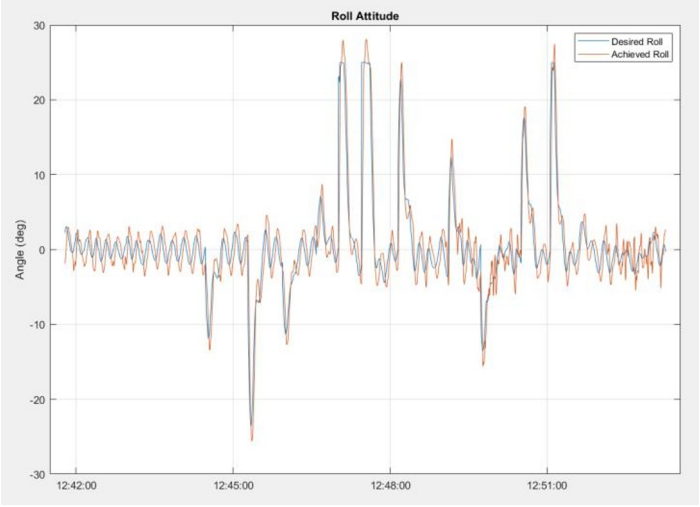

Fig. 15. Roll oscillations post tune.

5 Conclusion and recommendations

This research successfully demonstrated the integration and validation of a low-cost, open-source autopilot system for autonomous control of a full-sized motor glider. By retrofitting the Whisper airframe and following a structured methodology which included control force characterization, simulation-based tuning, and progressive in-flight testing, the system was configured to execute waypoint missions with reliable accuracy.

Simulation and flight results confirmed that the majority of tuning parameters carried over effectively from the SITL environment with only some adjustments required during full-scale testing. Autonomous mission performance improved steadily over successive flights. Final average path tracking and altitude errors reduced to 11.3 m and 28.7 m, respectively, with between-waypoint tracking errors as low as 1.75 m. While residual roll oscillations were noted in the logs, they were not perceptible in flight and were attributed to an overactive controller correcting minor disturbances that could have been managed by the airframe's inherent stability. Future work will refine I-gain tuning and address linkage variability to further mitigate this behaviour.

The system demonstrated sufficient authority and control precision to support high-endurance UAV applications. Future development should focus on the creation of custom control software tailored to the motor glider's aerodynamic behaviour, incorporating revised control loops that account for its inherent stability. Additionally, the refinement of mission planning tools to include airframe limitations such as climb rates, turn radii, and stall margins. These improvements would further enhance controller efficiency and ensure safer, more predictable autonomous operations. This study confirms the viability of adapting existing airframe for autonomous flight using open-source tools and highlights a practical pathway for developing affordable UAV platforms suited real-world missions.

References

1. Commission, N.P., *National Development Plan 2030: Our Future – Make it Work*. 2012, The Presidency, Republic of South Africa.
2. Department of Forestry, F. and t. Environment, *South Africa's Ocean Economy and Exclusive Economic Zone (EEZ)*. 2020, Republic of South Africa.
3. Schraader, L., *The impact of illegal fishing on south africa's economy*. 2013.
4. defenceWeb *Lack of SAAF aircraft a huge impediment to SA's search and rescue capabilities*. 2024.
5. Department of Defence, R.o.S.A., *South African Defence Review 2015*. 2015, Department of Defence.
6. News, N. *Safran's Patroller UAV proves its maturity during OCEAN2020*. 2021.
7. News, N. *MQ-9s Are Transforming Maritime Operations*. 2023.
8. Alqudsi, Y. and M. Makaraci, *UAV swarms: research, challenges, and future directions.* J. Eng. Appl. Sci, 2025. **72**(1): p. 12.
9. Sciences, A.F. *Centaur Optionally Piloted Aircraft System*. 2025; Available from: https://www.aurora.aero/centaur-optionally-piloted-aircraft/.
10. Laboratory, R.F.R. *Aircraft Assets | Capabilities*. 2025; Available from: https://www.raspet.msstate.edu/capabilities/aircraft-assets.
11. Sonex Aircraft, L. *MSU TEROS & Hurricane Helene*. 2018; Available from: https://www.sonexaircraft.com/msu-teros-hurricane-helene/.
12. AG, E.S. *ES15 Surveillance Aircraft Brochure*. 2019; Available from: https://gbaircraft.pl/wp-content/uploads/2019/05/ECARYS-Brochure_ES15.pdf.
13. Group, S. *PATROLLER™ RPAS*. 2021; Available from: https://www.safran-group.com/sites/default/files/2021-05/patroller-rpas.pdf.
14. Ebeid, E., et al., *A survey of open-source UAV flight controllers and flight simulators.* Microprocess Microsy, 2018. **61**: p. 11-20.
15. Koubaa, A., et al., *Micro Air Vehicle Link (MAVLink) in a Nutshell: A Survey.* arXiv preprint, 2019.
16. Team, A.D. *ArduPlane Documentation*. 2025; Available from: https://ardupilot.org/plane/index.html.
17. Park, S., J. Deyst, and J. How. *A new nonlinear guidance logic for trajectory tracking*. in *AIAA guidance, navigation, and control conference and exhibit*. 2004.
18. Project, P.A. *Getting Started with PX4 Autopilot | PX4 User Guide*. 2022; Available from: https://docs.px4.io/main/en/getting_started/.
19. Research, L. *How X-Plane Works*. 2025; Available from: https://www.x-plane.com/desktop/how-x-plane-works/.
20. Group, J.s.I. *Scheibe SF 25C Falke - All the World's Aircraft*. 2025; Available from: https://janes.migavia.com/deu/scheibe/sf-25c.html.
21. Technologies, L.H. *WESCAM MX-10: Intelligence, Surveillance and Reconnaissance (ISR) Imaging System*. 2025; Available from: https://www.l3harris.com/en/wescam-mx-10.
22. GmbH, B.-R. and C. KG, *Service Letter SL-912-016 R1: Performance and Manifold Pressure Data for ROTAX® Engine Type 912 S/ULS*. 2016, BRP-Rotax GmbH & Co KG.